Influence of Environment on the Antifolate Drug Trimethoprim: Energy Minimization Studies†

Cindy L. Fisher,‡ Victoria A. Roberts,§ and Arnold T. Hagler*,‖

The Agouron Institute, 505 Coast Boulevard South, La Jolla, California 92037, and Department of Molecular Biology, Research Institute of Scripps Clinic, La Jolla, California 92037

Received September 10, 1990; Revised Manuscript Received December 11, 1990

ABSTRACT: Environmental effects on trimethoprim (TMP), an inhibitor of bacterial dihydrofolate reductase (DHFR), were investigated with energy minimizations in vacuo, in the crystal, and in aqueous solution. The conformations, harmonic dynamics, and energetics of the antibacterial drug calculated in these environments were compared with each other and with those of two enzyme-bound drugs. Valence and torsion angles and their energies and overall intra- and intermolecular energies compensated one another in the minimized TMP structures. The conformations of the isolated and aqueous molecules were similar to that of TMP bound to chicken liver DHFR, while the structures from the TMP crystal and from the *Escherichia coli* DHFR complex were unique. Since neither the small-molecule crystal nor a local minimum of the isolated molecule gave the conformation of TMP bound to the bacterial enzyme, a combination of several experimental and theoretical techniques may be necessary to probe accessible conformations of a molecule.

Environment affects the structural, energetic, and dynamic properties of molecules. This presents difficulties in drug design, since the usual environments in which the structural properties of these molecules are studied experimentally (i.e., the solid state or solution) differ from the biologically significant state (bound to a receptor or enzyme). Understanding the nature of environmental effects on these properties is, therefore, essential. The abundance of experimental information in different environments for trimethoprim (TMP),[1] an inhibitor of dihydrofolate reductase (DHFR), makes it a good subject for studies of the influence of surroundings on structural properties. Several high-resolution crystal structures of TMP exist, both of the inhibitor alone as well as the binary complex of TMP bound to *Escherichia coli* DHFR and the ternary complex of TMP and the cofactor reduced nicotinamide adenine dinucleotide phosphate (NADPH) bound to chicken liver DHFR. In addition, TMP, which consists of a 2,4-diaminopyrimidine ring and a trimethoxyphenyl ring connected by a methylene group (see Figure 1), has the advantage of being a small molecule with only one major area of conformational freedom—the methylene group.

DHFR, a ubiquitous enzyme vital to all metabolic organisms, catalyzes the reduction of dihydrofolate to tetrahydrofolate using the cofactor NADPH. Because TMP binds much more tightly to bacterial DHFRs than vertebrate DHFRs, it selectively inhibits the action of the enzyme in bacteria and hence is used clinically as an antibacterial agent (Burchall & Hitchings, 1965; Baker, 1970; Baccanari et al., 1982). The vertebrate and bacterial DHFR crystal structures show a major difference in the conformations of the inhibitor (Matthews et al., 1985b). Thus, the conformational energetics of TMP may play an important role in its specificity and activity as an antibacterial agent. Understanding the source of the binding difference could lead to the design of more potent and selective antibacterial compounds. Previously, we had carried out a thorough comparison of our calculated model of the *E. coli* DHFR·TMP complex and the X-ray structure in order to test the validity of the model and to calculate the strain energy induced in the inhibitor upon binding (Dauber-Osguthorpe et al., 1988). We also compared the energetics of TMP in our models of the binary and ternary DHFR complexes from both *E. coli* and chicken liver to investigate the interaction energies of TMP with enzymes from different species (Roberts et al., 1986).

Here we report minimizations of TMP in a number of "environments"—in vacuo, in a small molecule crystal, and in aqueous solution—using minimization techniques to study the effects of surroundings on the conformation, strain energies, and harmonic dynamics of the inhibitor. To examine the accuracy of the force field used in these calculations, we compared the minimized small-molecule crystal structure with experiment. To examine the specific distortions induced in TMP upon binding to DHFR, the in vacuo, solvated, and small-molecule crystal minimizations were compared with those of the inhibitor bound to *E. coli* and chicken liver DHFRs. Finally, implications for drug design are discussed.

Experimental Procedures

System Setup. TMP has a pK_a of 7.5 in solution; the neutral molecule was therefore employed in the minimizations of the in vacuo, solvated, and small-molecule crystal models. Because the pyrimidine ring is probably protonated on N1 when bound to DHFR (Matthews et al., 1985a), the protonated molecule was used in the minimizations of the DHFR·TMP complexes described in previous work (Roberts et al., 1986; Dauber-Osguthorpe et al., 1988). Minimizations were carried out

† This work was supported by a grant from the National Institutes of Health (Grant GM 30564) and an NIH Postdoctoral Fellowship (Grant GM 11612 to C.L.F.). A grant of computer time on the Cray X-MP/48 at the San Diego Supercomputer Center was provided by the National Science Foundation (Grant PCM 8421273).

* To whom correspondence should be addressed.

‡ Present address: Department of Molecular Biology, Research Institute of Scripps Clinic, La Jolla, CA 92037.

§ Research Institute of Scripps Clinic.

‖ Present address: BIOSYM Technologies, Inc., 10065 Barnes Canyon Road, San Diego, CA 92121.

[1] Abbreviations: TMP, trimethoprim; DHFR, dihydrofolate reductase; NADPH, reduced nicotinamide adenine dinucleotide phosphate; RMS, root mean square.

0006-2960/91/0430-3518$02.50/0

using the Discover program (BIOSYM Technologies, Inc.) on a Cray X-MP/48 at the San Diego Supercomputer Center and on a VAX 11/785.

Two separate minimizations of TMP in vacuo were performed. In the first, the initial coordinates of TMP were taken from the binary *E. coli* DHFR crystal structure (Bolin et al., 1982). Hydrogen atoms were added in standard geometries. In the second minimization, coordinates were taken from the high-resolution neutron diffraction structure of neutral TMP (Koetzle & Williams, 1976), which includes hydrogen atom positions.

The solvated model was also constructed from the neutron diffraction TMP structure. Water molecules filling a 30-Å cube at a density of 1 g mL^{-1} were subjected to 4 ps of molecular dynamics to equilibrate the system partially. TMP was placed into the center of this cube and all waters that were involved in a steric overlap with the inhibitor were removed. The resultant system contained one TMP molecule and 846 water molecules.

To construct the TMP small-molecule crystal system, a crystal (containing two symmetry-related molecules of TMP) was generated with dimensions of a = 10.523 Å, b = 11.222 Å, c = 8.068 Å, α = 101.22°, β = 112.15°, and γ = 112.65° and with $P\bar{1}$ symmetry. The relevant periodic boundary conditions determined by the unit cell vectors were applied. In this structure, hydrogen bonds exist between the two pyrimidine rings of the two TMP molecules. To avoid potential errors in calculating the strong electrostatic forces between charged molecules and counterions (Avbelj et al., 1990), this neutral TMP crystal structure was used rather than other protonated and derivatized TMP crystal structures that have been solved (Phillips & Bryan, 1969; Oberhänsli, 1970; Koetzle & Williams, 1978; Cody, 1984).

Minimization Procedure. The potential energy of the system was calculated from a valence force field represented by an analytical function (Hagler, 1985; Dauber-Osguthorpe et al., 1988). A dielectric constant of one was used. Partial charges used for the neutral TMP minimizations are shown in Figure 1, and the remaining parameters are published elsewhere (Dauber-Osguthorpe et al., 1988).

The two TMP models in vacuo were minimized by using the conjugate gradient method (Fletcher & Reeves, 1964) until the maximum derivative was less than 1×10^{-5} kcal mol^{-1} $Å^{-1}$, giving an average derivative of 2×10^{-6} kcal mol^{-1} $Å^{-1}$. No cutoff distance was applied to nonbonded interactions.

Periodic boundary conditions were used to simulate the environment for the solvated and small-molecule crystal TMP models. A cutoff distance of 15 Å, shown to be a reasonable tradeoff between accurate representation of energies and computational time (Kitson & Hagler, 1988a), was used with a continuous switching function applied from 13 to 15 Å (Swope et al., 1982) to taper off interactions gradually. The solvated model was minimized first with the steepest descent algorithm (Cauchy, 1847) until the maximum derivative was less than 20 kcal mol^{-1} $Å^{-1}$ and then with the conjugate gradient algorithm (Fletcher & Reeves, 1964) to a maximum derivative of less than 1×10^{-3} kcal mol^{-1} $Å^{-1}$ and an average derivative of 3×10^{-5} kcal mol^{-1} $Å^{-1}$. The small-molecule crystal model was minimized first with 100 steps of the steepest descent method to a maximum derivative of less than 10 kcal mol^{-1} $Å^{-1}$ and then with a quasi-Newton algorithm (Fletcher, 1970), resulting in a maximum derivative of less than 5×10^{-6} kcal mol^{-1} $Å^{-1}$ and an average derivative of 6×10^{-7} kcal mol^{-1} $Å^{-1}$. The intermolecular energies for the small-molecule crystal and solvated systems were calculated with the 15-Å cutoff

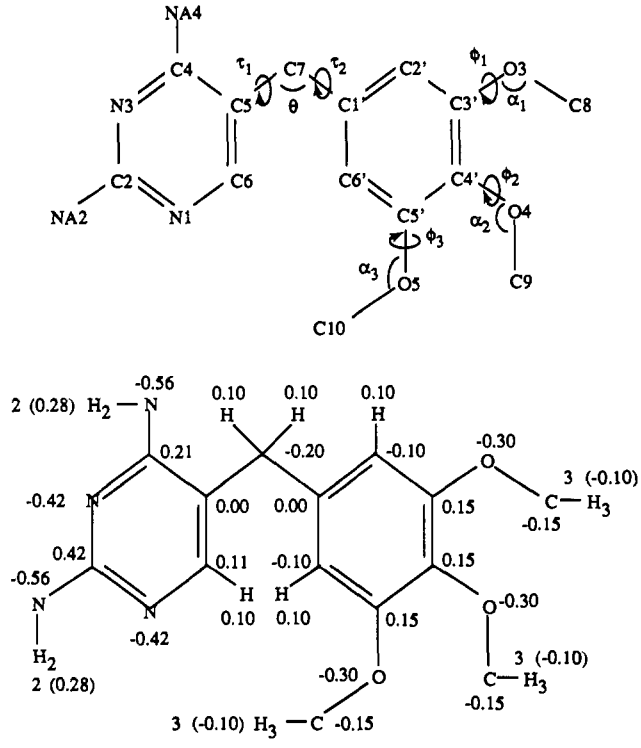

FIGURE 1: Structure of trimethoprim. The top figure shows the torsion angles τ_1(C4–C5–C7–C1′) and τ_2(C5–C7–C1′–C2′) about the central methylene carbon, C7, and ϕ_1(C_2′–C3′–O3–C8), ϕ_2(C3′–C4′–O4–C9), and ϕ_3(C4′–C5′–O5–C10) about the three methoxy groups. Valence angles θ(C5–C7–C1′), α_1(C3′–O3–C8), α_2(C4′–O4–C9), and α_3-(C5′–O5–C10) are also shown. Partial charges used in the present simulation are given next to each atom in the bottom figure.

distances used in the minimizations.

Vibrational Frequency Calculations. Vibrational frequencies were calculated from the second derivatives of the energy of the structures of TMP (Hagler, 1985). The frequencies of the in vacuo and small-molecule crystal inhibitors were calculated directly from the structures obtained as described above. The solvated system was further minimized by fixing all water molecules greater than 3.3 Å from any inhibitor atom and continuing minimization until the maximum derivative in energy was less than 5×10^{-5} kcal mol^{-1} $Å^{-1}$, allowing for coupling of the TMP frequencies with the immediate aqueous environment. Frequencies for TMP in the *E. coli* DHFR complex were determined from mass-weighted second derivatives of the structure obtained by starting with the system minimized as outlined below, removing the proton on N1 to allow for a direct comparison with the other systems, fixing the positions of the protein atoms, and further minimizing the inhibitor until the maximum derivative was less than 5×10^{-5} kcal mol^{-1} $Å^{-1}$.

Enzyme Complex Simulations. The minimized TMP structures generated previously for the *E. coli* DHFR binary (V. A. Roberts, C. L. Fisher, and A. T. Hagler, unpublished results) and chicken liver DHFR ternary (Roberts et al., 1986) complexes were used in this work. For these minimizations, the initial coordinates were taken from the crystal structures of *E. coli* DHFR binary and chicken liver DHFR ternary complexes. Crystallographically determined water molecules within 7 Å of the TMP and NADPH and waters that appeared to play a structural role in the protein were included. All hydrogen atoms were added in standard geometries, with TMP protonated on N1. Water molecules were added to solvate the active site, the cofactor NADPH (or the NADPH site in the binary system), and all charged groups on the surface of the protein. The partially solvated protein complex was treated

Table I: RMS Deviations of Trimethoprim between Experimental and Minimized Crystal Structures (in angstroms)[a]

	TMP crystal	*E. coli* DHFR binary	chicken liver DHFR ternary
pyrimidine	0.11 (0.13)	0.24 (0.25)	0.22 (0.27)
methylene	0.07 (0.07)	0.29 (0.29)	0.11 (0.11)
trimethoxyphenyl	0.13 (0.22)	0.20 (0.47)	0.18 (0.41)
overall	0.12 (0.18)	0.23 (0.40)	0.19 (0.36)

[a] Deviations based on fit of the 13 non-hydrogen ring atoms and methylene carbon. Reported deviations are for these atoms. Parenthetical values represent deviations for all 21 non-hydrogen atoms.

Table II: Comparison of Selected Valence and Torsion Angles of Experimental and Minimized Conformations of Trimethoprim

	TMP crystal[a]		bound in *E. coli* DHFR binary[b]		bound in chicken liver DHFR ternary[b]	
angle	exptl	calcd	exptl	calcd	exptl	calcd
τ_1(C4–C5–C7–C1′)	−89	−95	180	−162	−84	−95
τ_2(C5–C7–C1′–C2′)	153	143	75	65	110	101
θ(C5–C7–C1′)	118	119	108	119	110	114
ϕ_1(C2′–C3′–O3–C8)	−5	2	16	6	−21	47
ϕ_2(C3′–C4′–O4–C9)	−101	−116	65	160	−139	−108
ϕ_3(C4′–C5′–O5–C10)	−172	−160	159	164	169	−129
α_1(C3′–O3–C8)	118	125	134	124	119	121
α_2(C4′–O4–C9)	115	119	111	125	123	119
α_3(C5′–O5–C10)	118	124	142	125	122	121

[a] The second molecule in the unit cell is symmetry-related; thus, its torsion angles are equal but of opposite sign. [b] From system minimized with protonated trimethoprim.

as a system in vacuo in all cases, with no cutoff distances or periodic boundary conditions applied. The structures were minimized to a maximum derivative of less than 0.025 kcal mol^{-1} Å^{-1}.

Results

Comparison of Experimental with Minimized Structures. Root-mean-square (RMS) deviations of atomic positions (Table I) and valence and torsion angles (Table II) indicate the structural differences between TMP in the three experimental crystal systems and the three corresponding minimized structures (Figure 2). To calculate the RMS deviations for TMP, the minimized structure was superimposed onto the experimental structure with a least-squares fit of the structural backbone—the methylene carbon and the six non-hydrogen atoms of each of the two rings. Given this fit, RMS deviations were calculated separately for the fitted atoms and for all non-hydrogen atoms.

The major area of mobility in the conformation of TMP is reflected in the torsion angles τ_1 and τ_2 and the valence angle θ about the central methylene group (see Figure 1). These angles define the relative orientation of the two aromatic rings. The orientation of the three methoxy groups, which are also mobile, are represented by the torsions ϕ_1, ϕ_2, and ϕ_3 and the valence angles α_1, α_2, and α_3.

The smallest deviation of a minimized structure from its experimental structure was found for TMP from the small-molecule crystal, with an RMS deviation between their structural backbones of 0.12 Å (Table I). The larger RMS deviation between all non-hydrogen atoms of these two structures was predominantly due to the methoxy groups (A in Figure 2). The small RMS deviations between the structural backbones corresponded to torsion angle deviations of 6° for τ_1 and 10° for τ_2 (Table II). Angular deviations in the methoxy groups were somewhat larger (7–15°).

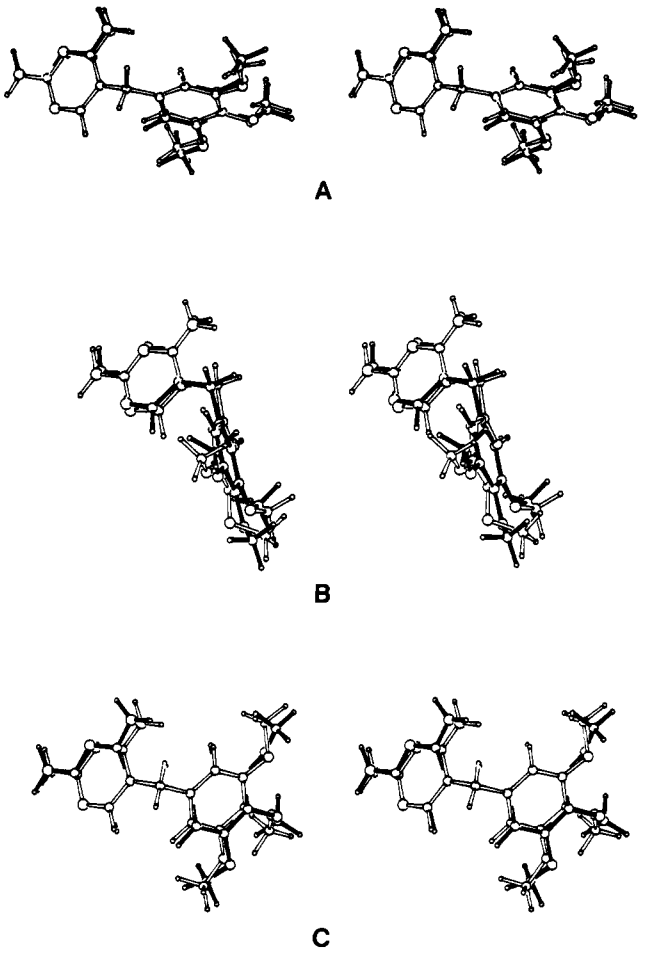

FIGURE 2: Stereo pairs showing the fit of experimental (solid bonds) to calculated (open bonds) trimethoprim structures. The fit of TMP from the minimized TMP crystal to the initial structure is shown in part A, of TMP in the *E. coli* DHFR complex in part B, and of TMP in the chicken liver DHFR complex in part C.

Larger RMS deviations between experimental and minimized TMP structures were found for the enzyme models, with greater RMS deviations in the *E. coli* DHFR binary complex than in the chicken liver DHFR ternary complex (Table I). In both enzyme-bound cases (B and C in Figure 2), the three methoxy groups of the trimethoxyphenyl moiety were again found to be responsible for the larger RMS deviations between all non-hydrogen atoms. The RMS deviations for the *E. coli* DHFR system corresponded to differences of up to 17° in the valence angles and 95° in the torsion angles (Table II). Less drastic movements in the valence angles (about 4°) were found in TMP from the chicken liver DHFR complex, but there was still a difference of 62° in the torsion ϕ_3. As discussed below, errors in the experimental structures give rise to a significant contribution to these large deviations.

Effect of Environment on Minimized Conformations. TMP was minimized in six environments: two in vacuo, one solvated, one in the small-molecule crystal, and two bound to enzymes. Here, we compare the resultant minimized structures.

Two separate minimizations of TMP in vacuo were performed, one starting from the small-molecule crystal coordinates and the other starting from the TMP coordinates of the *E. coli* DHFR binary complex. The initial RMS deviation between the structural backbones of the two was 1.09 Å. Upon minimization, the two structures were virtually identical, with an RMS deviation of only 0.01 Å (Table III). The torsion angles for the three methoxy groups showed the only significant difference. While the torsion angles of the two meta sub-

Table III: RMS Deviations between Heavy Atoms of Minimized Trimethoprim Structures in Various Environments (in angstroms)[a]

	isolated from *E. coli* DHFR	solvated from TMP crystal	TMP crystal	*E. coli* DHFR binary	chicken liver DHFR ternary
isolated from TMP crystal	0.01 (0.54)	0.20 (0.51)	0.57 (1.11)	0.70 (1.15)	0.16 (0.51)
isolated from *E. coli* DHFR		0.20 (0.67)	0.57 (1.17)	0.69 (1.03)	0.16 (0.69)
solvated from TMP crystal			0.38 (0.68)	0.79 (1.36)	0.05 (0.23)
TMP crystal				1.03 (1.85)	0.42 (0.69)
E. coli DHFR binary					0.76 (1.41)

[a] Deviations based on fit of the 13 non-hydrogen ring atoms and methylene carbon. Reported deviations are for these atoms. Parenthetical values represent deviations for all 21 non-hydrogen atoms.

Table IV: Comparison of Selected Valence and Torsion Angles of Minimized Conformations of Trimethoprim in Various Environments (in degrees)

	isolated from					
angle	*E. coli* DHFR	crystal	solvated	TMP crystal[a]	*E. coli* DHFR[b] binary	chicken liver DHFR[b] ternary
τ_1(C4–C5–C7–C1′)	−94	−94	−94	−95	−162	−95
τ_2(C5–C7–C1′–C2′)	87	87	106	143	65	101
θ(C5–C7–C1′)	112	112	114	119	119	114
ϕ_1(C2′–C3′–O3–C8)	−7	−1	25	2	6	47
ϕ_2(C3′–C4′–O4–C9)	92	−92	142	−116	160	−108
ϕ_3(C4′–C5′–O5–C10)	−175	−180	160	−160	164	−129
α_1(C3′–O3–C8)	125	125	124	125	124	121
α_2(C4′–O4–C9)	117	117	123	119	125	119
α_3(C5′–O5–C10)	125	125	124	124	125	121

[a] The second molecule in the unit cell is symmetry-related; thus, its torsion angles are equal but of opposite sign. [b] From system minimized with protonated trimethoprim.

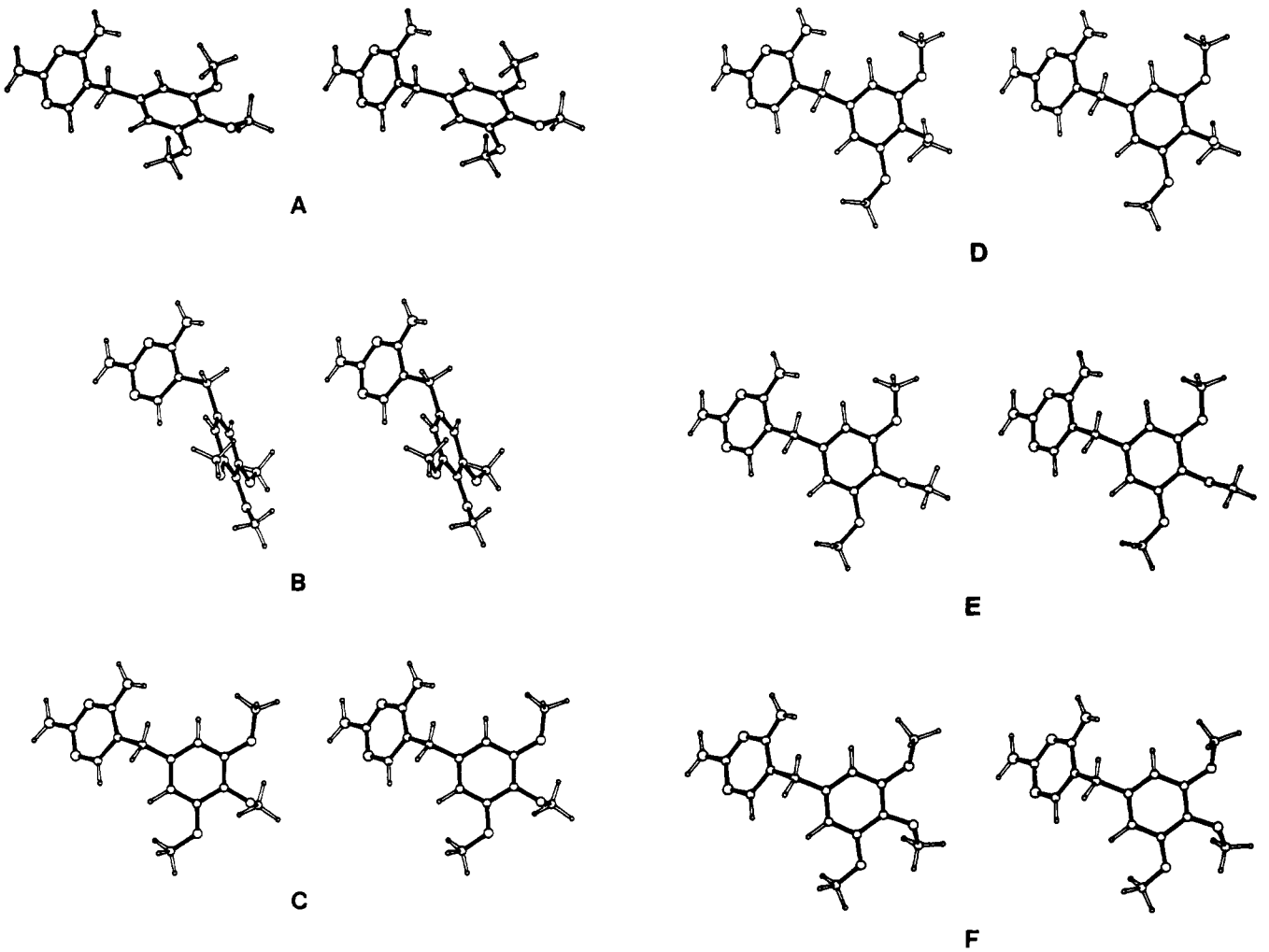

FIGURE 3: Stereo pairs of the conformations of trimethoprim from minimizations. The conformation from the TMP crystal is shown in part A, the *E. coli* DHFR binary complex in part B, and the chicken liver DHFR ternary complex in part C. The two conformations from the in vacuo minimizations starting from the TMP crystal and the *E. coli* binary complex structures are shown in parts D and E, respectively, and the solvated structure is shown in part F.

Table V: Energies of Neutral Trimethoprim in Minimized Systems

energies		isolated from					
		E. coli DHFR	crystal	solvated	TMP crystal	*E. coli* DHFR[a] binary	chicken liver DHFR[a] ternary
valence	bond	27.9	27.9	28.4	25.8	28.8	26.9
	valence angle (θ)	15.3	15.3	16.9	15.7	20.2	12.7
	torsion angle (ϕ)	7.2	7.1	6.9	8.8	2.8	16.4
	out of plane	0.0	0.0	0.0	0.0	0.0	0.0
	cross terms	1.9	1.9	2.2	1.9	2.4	1.8
	total valence	52.3	52.2	54.4	52.3	54.2	57.8
nonbond	van der Waals	76.3	76.3	77.8	82.4	82.0	76.6
	Coulombic	−75.0	−75.1	−75.7	−75.7	−76.5	−75.9
	total nonbond	1.3	1.2	2.1	6.6	5.5	0.7
total intramolecular		53.6	53.4	56.4	59.0	59.8	58.5
intermolecular	van der Waals			−16.2	−39.0	−28.1	−32.1
	Coulombic			−17.5	−10.4	−14.7	−9.7
total intermolecular				−33.7	−49.4	−42.8	−41.8
overall total		53.6	53.4	22.7	9.5	17.0	16.7

[a] From system minimized with protonated trimethoprim; energies calculated with unprotonated molecule.

stituents differed by no more than 6° from one minimized structure in vacuo to the other (Table IV), those of the para methoxy groups differed by about 180°; i.e., the para methoxy groups were on opposite sides of the ring (E and F in Figure 3), resulting from an energy barrier to rotation past the plane of the ring. Dependence on the starting conformation was confirmed by repeating the minimization of TMP in vacuo starting with the X-ray structure of TMP from the *E. coli* DHFR complex with the torsion of the para methoxy forced to a value 180° opposite from the original. The resulting structure from this minimization was identical with that from the in vacuo minimization starting from the small-molecule crystal structure, demonstrating the convergence properties of the minimizer.

The TMP structures from the minimized chicken liver DHFR complex (C in Figure 3) and the solvated (D) and in vacuo (E, F) structures were similar. The RMS deviations (Table III) of the structural backbone of TMP among these three structures (0.05–0.20 Å) were comparable with the small deviations seen between the experimental and minimized structures of the small-molecule crystal (0.18 Å). These deviations were reflected in small variations of τ_1 and τ_2: −95° and 101° for TMP in the chicken liver DHFR complex versus −94° and 87° for the inhibitor in vacuo and −94° and 106° for the solvated molecule (Table IV). The larger differences in methoxy torsion angles (Table IV) were once again responsible for the larger overall RMS deviations (Table III) among these four TMP structures (0.23–0.69 Å).

The TMP conformations in the small-molecule crystal and the *E. coli* DHFR complex (A and B in Figure 3) were each unique. The RMS deviations of the structural backbone between TMP in the small molecule crystal and all other systems varied from 0.38 to 1.03 Å, with the same τ_1 value (−95°) as the systems described above but a τ_2 value (143°) that led to a different conformation. For TMP in the *E. coli* DHFR complex, the differences were even more apparent. The RMS deviations of the structural backbone varied from 0.69 to 1.03 Å. Although the τ_2 value (65°) was close to that found in the systems in vacuo, the τ_1 value (−162°) clearly indicated a distinct conformation from that of any other system.

Effect of Environment on Energetics. The differences and similarities in the conformations of neutral TMP in the in vacuo, small-molecule crystal, solvated, and enzyme-bound forms were reflected in the final values of the intra- and intermolecular energies for the minimized molecule in the context of its surroundings. In Table V, the strain energies for the minimized structures are given, as well as the energy contributed by the environment that stabilizes the strained conformation, broken down into the various components that contribute to the overall total energy. The difference between the lowest and highest intramolecular energies was only 6.3 kcal mol^{-1}, demonstrating that there were several conformations accessible to the molecule within this energy range. The intermolecular energies in the nonisolated systems compensated for the intramolecular strain induced by the surroundings, demonstrating that the environment strongly influences the overall energetics of the molecule (Roberts et al., 1986; Kitson & Hagler, 1988a).

(*a*) *Distribution of Strain Energies.* Inspection of the intramolecular energetics for TMP revealed how specific energy components are affected by the environment (Table V). For example, an interplay of the valence angle and torsion angle energies of TMP could be seen. In each system, a less favorable, or higher, total valence angle energy for TMP accompanied a more favorable, or lower, torsion angle energy. The methoxy groups of the trimethoxyphenyl moiety were responsible for this difference in distribution of valence and torsion angle energies. The two molecules in vacuo and the small-molecule crystal structure had similar values for these two energies. Examination of the valence and torsion angles of the methoxy groups for these systems showed them to be nearly identical, with the meta methoxy groups near the plane of the aromatic ring and the para methoxy group approximately perpendicular to it (Table IV). The solvated molecule had a somewhat higher valence angle energy and a slightly lower torsion angle energy due to the twist of the para methoxy group closer to the plane of the aromatic ring (ϕ_2 = 142°). The *E. coli* DHFR binary system with its para methoxy group almost in the plane of the ring (ϕ_2 = 160°) and corresponding large valence angle (α_2 = 125°) had the most favorable torsion energy (2.8 kcal mol^{-1}) and the least favorable valence angle energy (20.2 kcal mol^{-1}). In contrast, the para methoxy group of TMP in the chicken liver DHFR ternary complex had valence and torsion angles similar to those found in the in vacuo and small-molecule crystal systems, but the two meta methoxy groups were tipped further out of the plane of the ring than those found in any of the other situations (ϕ_1 = 47°, ϕ_3 = −129°). This resulted in less strained valence angles, causing a lowering of the valence angle energy (12.7 kcal mol^{-1}) and a dramatic increase in the torsion angle energy (16.4 kcal mol^{-1}). Therefore, as the methoxy groups moved into the plane of the aromatic ring, the valence angles and energies increased while the torsion angles and energies decreased.

A second compensatory effect was seen in the overall valence and nonbond energies in the small-molecule crystal and en-

Table VI: N-H Hydrogen Bonds and Stretching Frequencies in Minimized Neutral Trimethoprim Systems

		frequency (cm^{-1})[a]		hydrogen bond			
bonds	system	anti	sym	dist (Å)	acceptor	dist (Å)	acceptor
H-NA2-H	isolated	3606	3487				
	solvated[b]	3582	3458	2.5	water O	3.3	water O
	TMP crystal	3586	3453	2.3	N1	2.6	O3
	E. coli DHFR[c]	3503	3366	1.8	Asp^{27} COO^-	2.0	water O
H-NA4-H	isolated	3580	3464				
	solvated[b]	3501	3393	2.1	water O	2.2	water O
	TMP crystal	3574	3461	2.1	N3	2.6	N1
	E. coli DHFR[c]	3551	3426	1.9	Ile^5 C=O	2.4	Ile^{94} C=O

[a] Anti = antisymmetric N-H stretch; sym = symmetric N-H stretch. [b] Calculated with waters within 3.3 Å allowed to move. [c] Calculated with protein atom positions held fixed.

zyme-bound structures. The van der Waals energies in the small-molecule crystal and *E. coli* DHFR systems were considerably higher than that in the chicken liver DHFR complex. These higher energies were compensated for by lower total valence energies than found in the chicken liver DHFR system, arising from lower bond and torsion energies in the small-molecule crystal and a lower torsion energy in the *E. coli* DHFR complex. Thus, in the highly restrictive small-molecule crystal and enzyme-bound environments there was a direct correlation between valence and nonbond energetics, where the increase in one was compensated for by a decrease in the other, bringing the intramolecular energies of all three systems to within 1 kcal mol^{-1} of one another.

(*b*) *Intermolecular Energetics.* Interaction of a molecule with its environment is evidenced in the intermolecular energies, arising from van der Waals and Coulombic interactions, between the molecule and its surroundings. In these studies, the major contributor to the overall intermolecular energetics (excluding TMP in vacuo from this discussion) was the van der Waals interaction term, which ranged from −39.0 to −16.2 kcal mol^{-1} (Table V). The small-molecule crystal system had the most favorable van der Waals energy, since it is a highly compact environment. In effect, TMP solvated itself in the crystal and had the same amount of hydrophobic and hydrophilic surface as its "solvent". The second most favorable intermolecular van der Waals energy was seen in the chicken liver DHFR ternary complex, where the protein surrounds much of the trimethoxyphenyl group (Roberts et al., 1986). In the *E. coli* DHFR complex, the trimethoxyphenyl moiety extends out into a water-filled cavity leading to the protein surface, such that one face of the ring is exposed to solvent. This gave rise to a less favorable van der Waals energy than in the chicken liver DHFR system. The solvated molecule, where hydrophobic contacts were at a minimum, had the least favorable van der Waals energy.

Compensatory effects were found in the van der Waals and Coulombic energies. When a system had a relatively unfavorable van der Waals energy, the corresponding Coulombic energy tended to be more favorable. The inhibitor in the chicken liver DHFR complex and in the small-molecule crystal had the least favorable electrostatic energies. In these two cases, there were not as many hydrogen bonds to polar groups as there are in the *E. coli* DHFR complex (Dauber-Osguthorpe et al., 1988) or the solvated system. The solvated TMP had the most favorable electrostatic energy. This was insufficient to counteract the lack of hydrophobic interactions, however, as indicated by the higher van der Waals energies. Thus, its overall intermolecular energy was the least favorable.

Effect of Environment on Harmonic Dynamics. Involvement of an NH group in a hydrogen bond weakens (lengthens) the covalent N-H bond, which in turn lowers the stretching frequency of the bond. Environmental effects on the vibrational frequencies in TMP correlated with the strength of the hydrogen bonds involved.

Table VI gives the frequencies and hydrogen bond distances of the symmetric and antisymmetric N-H stretches found for the two NH_2 groups of TMP in the in vacuo, small-molecule crystal, solvated, and *E. coli* DHFR-bound environments. For both amino groups, the frequencies in vacuo were the highest, as expected, since these hydrogens were not involved in any hydrogen bonds. The NH_2 groups in the small-molecule crystal were involved in four long hydrogen bonds. Furthermore, nitrogen atoms, which form weaker hydrogen bonds than oxygen atoms, acted as the acceptors for three of these hydrogen bonds. Thus, there was little effect on the stretching frequencies (no more than 30 cm^{-1} compared to the values in vacuo). For solvated TMP, the NA2 amino group was again involved in long hydrogen bonds with only slight effects on the frequencies. The NA4 group, however, participated in stronger hydrogen bonds, giving rise to decreases in the symmetric and antisymmetric stretching frequencies of 79 and 71 cm^{-1}, respectively. In the *E. coli* DHFR complex, the most pronounced shifts occurred in the stretching frequencies of the NA2 hydrogens, where there were short hydrogen bonds with a carboxylate oxygen of Asp^{27} and with a water oxygen. This caused decreases of 103 cm^{-1} in the symmetric and 121 cm^{-1} in the antisymmetric frequencies relative to the molecule in vacuo. The NA4 hydrogens formed hydrogen bonds with two backbone carbonyl oxygens, which were involved in interactions with other parts of the enzyme and not optimally aligned for overlap. Thus, the frequencies of these hydrogens were lower than those of the small-molecule crystal, but not as low as for the solvated TMP, in which the alignments of the hydrogen-bonded water oxygens were more ideal.

Discussion

Analysis of Methodology. The comparison of the high-resolution neutron diffraction crystal structure of TMP with the calculated crystal provides an excellent test of potential parameters [Figure 2 and Dauber-Osguthorpe et al. (1988)]. The small RMS and angle deviations that resulted (Tables I and II) justify extending the application of the parameters to the modeling of enzyme-bound TMP.

R factors reflect the uncertainty of atomic positions for crystal structures. The *R* factors for the *E. coli* DHFR complex, 0.19 at 2.3-Å resolution, and the chicken liver DHFR complex, 0.22 at 2.2-Å resolution (Matthews et al., 1985a), are an order of magnitude larger than the *R* factor of 0.013 for the small-molecule crystal (Koetzle & Williams, 1976). Small errors in atomic positions can lead to large deviations in angles and corresponding artifactually large energies. For example, in the *E. coli* DHFR system, the uncertainty in atomic positions results in overly large valence angles (134° and 142°) for the two meta methoxy groups, which are the

Table VII: Valence and Torsion Angles for the Methylene Group of Trimethoprim and Analogues[a]

	compound	θ	τ_1	τ_2	ref
1.	trimethoprim	118	−89	153	Koetzle & Williams, 1976
2.	diaveridine	115	−66	155	Koetzle & Williams, 1978
3.	TMP-1-oxide	117	−69	151	Oberhänsli, 1970
4.	methoxycarbonyl TMP deriv (molec 1)	116	74	29	Cody, 1984
	methoxycarbonyl TMP deriv (molec 2)	116	70	46	Cody, 1984
5.	TMP·diethylbarbituric acid	116	84	168	Shimizu et al., 1982
6.	TMP·HBr	112	158	112	Phillips & Bryan, 1969
7.	isopropenyl TMP derivative·$CH_3CH_2SO_3H$	114	153	98	Cody, 1984
8.	TMP·sulfamethoxazole	114	173	88	Giuseppetti et al., 1980
9.	TMP·benzisothiazolone dioxide	110	−68	122	Shimizu & Nishigaki, 1982
10.	chicken liver DHFR·TMP·NADPH	110	−85	102	Matthews et al., 1985a
11.	*E. coli* DHFR·TMP	108	177	76	Matthews et al., 1985a

[a] Adapted from Matthews et al. (1985b).

main contributors to the high valence angle energies in the unminimized X-ray structure (49.3 kcal mol^{-1} for *E. coli* DHFR compared with 14.7 kcal mol^{-1} for the small-molecule crystal). These large angular distortions are also reflected in the large changes found in these valence angles upon minimization (Roberts et al., 1986).

The large change upon minimization in the para methoxy group of TMP from the *E. coli* DHFR complex might also be due to the method in which the initial system was constructed. The X-ray structure of the *E. coli* DHFR binary system contains two nonidentical complexes, complexes I and II, in the asymmetric unit (Matthews et al., 1985a). The protein coordinates of complex II are the better defined of the two, but the para methoxy group of TMP in complex II lies in the plane of the trimethoxybenzene ring, which is unusual when compared to NMR and small-molecule crystal structures. The TMP in complex I had a more normal para methoxy torsion angle. Thus, when constructing the enzyme for minimizations, the protein coordinates from complex II and the inhibitor coordinates from complex I were used (V. A. Roberts, C. L. Fisher and A. T. Hagler, unpublished results). Upon minimization, however, the para methoxy group of TMP was pushed back into the plane of the benzene ring, as observed in the experimental structure, by its environment—the backbone between Ser^{49} and Ile^{50} of the αC helix of the DHFR and two crystallographically determined waters near the active site. Thus, the minimized model reflected the energetic preference of TMP to have its para methoxy group in the plane of the aromatic ring when bound to DHFR in the conformation found in complex II.

Interplay between Intramolecular Components. (*a*) *Valence and Torsion Angles of the TMP Methylene Group.* The relative orientation of the pyrimidine and trimethoxyphenyl rings of TMP depends on the torsion angles τ_1 and τ_2 and the valence angle θ around the methylene group (Cody, 1984). The three general orientations in crystal structures of TMP and structural analogues (see Table VII) show the correlation between the torsion angles and the valence angle. In the first, the edge of the trimethoxyphenyl ring points toward the center of the pyrimidine ring (entries 1–5 in Table VII), resulting in the largest values of θ (115–118°). The crystal structure of neutral TMP is in this category (A in Figure 2). In the second orientation, the edge of the pyrimidine ring points toward the center of the trimethoxyphenyl ring (entries 6–8 in Table VII), also found in TMP from the *E. coli* DHFR X-ray structure (B in Figure 2). These structures have lower θ values (112–114°). The final orientation places the planes of the pyrimidine and phenyl rings facing one another (entry 9 in Table VII), which has the lowest value of θ at 110°. This orientation is also seen in TMP from the chicken liver DHFR X-ray structure (C in Figure 2).

The correlation between τ_1 and τ_2 and θ was also seen in the minimized structures (Table IV). When the values of τ_1 and τ_2 were around ±90°, as in the minimized in vacuo, solvated, and chicken liver DHFR-bound TMPs, θ was smaller (112–114°). If either or both torsions moved away from ±90°, θ became larger. In the *E. coli* DHFR-bound inhibitor, the edge of the pyrimidine ring pointed almost directly at the center of the trimethoxyphenyl ring, resulting in a larger θ value (119°). In the small-molecule crystal, the edge of the trimethoxyphenyl ring pointed toward the face of the pyrimidine ring, again resulting in a large θ (119°). This effect stems from the increased van der Waals repulsion when either of the two rings turns in toward the other.

(*b*) *Valence and Torsion Angles of the Methoxy Groups.* The preferred conformation of the three methoxy groups—defined by torsion angles, ϕ_1, ϕ_2, and ϕ_3 and valence angles α_1, α_2, and α_3—depends on their placement on the aromatic ring. For a single methoxy group (e.g., anisole), the methyl group prefers to lie in the plane of the ring, allowing delocalization of the nonbonding electrons of the oxygen atom into the π orbitals of the aromatic ring. Because of steric interactions of the methyl group with a neighboring hydrogen atom on the ring, the valence angle of the methoxy group is larger than ideal. If the methyl group is out of the plane, the delocalization of the oxygen lone pairs is disrupted, but the valence angle is not affected by steric hindrance with the ring and is closer to its ideal value. In crystal structures of TMP derivatives (Oberhänsli, 1970; Koetzle & Williams, 1976; Giuseppetti et al., 1980; Shimizu & Nishigaki, 1982; Shimizu et al., 1982) and in the solution structure of trimethoxybenzene from ^{13}C NMR (Makriyannis & Fesik, 1982), the two meta methoxy groups tend to lie in the plane of the aromatic ring pointing away from the para methoxy group, resulting in ϕ_1 and ϕ_3 values close to either 0° or 180°. Values for ϕ_2 indicate that the para methoxy group prefers to lie out of the plane of the ring for steric reasons. Correspondingly, values for α_1, α_2, and α_3 follow a general pattern based on the torsion angles—the closer the methoxy group is to the plane of the phenyl, the larger its valence angle.

In our minimizations, the orientations of the three methoxy groups depended greatly on their environment. In vacuo, since there was no external environment to perturb the preferred orientations for the molecule, the conformations of the methoxy substituents were consistent with NMR and crystallographic results: the two meta groups lay in the plane of the aromatic ring, while the para methoxy group pointed out of the plane. Likewise, the minimized small-molecule crystal and solution structures showed the same trends, although the torsion angles were less "ideal" than for the molecule in vacuo. On the other hand, in the enzyme-bound TMPs, interactions with the protein altered the orientation of the methoxy groups considerably.

In the chicken liver DHFR complex, the protein surrounded the meta groups, forcing them into a nonplanar orientation. In the *E. coli* DHFR binary system, the para methoxy group was forced into the plane of the aromatic ring by the enzyme, as discussed above.

(*c*) *Valence and Torsion Angle Energies.* Correlations between the valence and torsion angle values were reflected in the overall valence angle and torsion angle energies in the minimized structures. Compensation of valence and torsion angle energies was most important in the DHFR complexes where the enzyme strongly constricts the placement of the methoxy groups. TMP compensated by adjusting the methyl group positions to achieve a balance between valence and torsion angle energies. If the valence angles were fixed, these compensatory effects would not have been seen, resulting in unrealistic energies. This underscores the need to include valence angles in the force field description, as strain is distributed over all degrees of freedom.

The Balance between Intra- and Intermolecular Forces. The intramolecular strain energies of the minimized TMP in the various states followed the order: in vacuo < solvated < small-molecule crystal ≈ enzyme bound. Because the molecule in vacuo was free to adopt any conformation unfettered by its surroundings, it adopted that conformation with the most favorable intramolecular energy. The water network about the solvated TMP molecule, which is intermediate between the in vacuo and small-molecule crystal environments in its constraint on TMP, induced about 3 kcal mol^{-1} of strain energy in the inhibitor. The small-molecule crystal and enzyme-bound environments induced about the same amount of strain energy on the inhibitor—from 5.0 to 6.3 kcal mol^{-1} (Table V), even though the TMP conformations in these three systems were quite different from one another. Thus, the ordering of intramolecular energies reflected the degree of constraint imposed by the external system on the inhibitor in each environment.

In addition to the compensatory effects seen in the individual terms that contribute to the total intra- or intermolecular energy, there was an interplay seen between these two energies as well. The aqueous environment both induced less strain on and had the least favorable intermolecular interactions with TMP, supporting the preference of TMP for a more hydrophobic environment. The strain energy induced in the inhibitor upon binding to the enzyme, a partially solvated environment, was comparable with that induced in the crystal. In the anhydrous small-molecule crystal of TMP, however, intermolecular interactions greatly stabilized the structure, giving the small molecule crystal system the lowest overall energy of all those studied. Thus, the crystal environment behaved as a receptor much as the DHFR enzyme did, forcing the molecule into an energetically strained conformation, but compensating by favorable intermolecular interactions. A similar effect is seen in calculations on a peptide in its crystal environment (Kitson & Hagler, 1988a,b) and in DHFR minimizations (Roberts et al., 1986).

Implications for Drug Design. The conformations found for the minimized structures (Table IV) have significant implications regarding drug design and receptor modeling. One might ask if the minimized structure of a drug in any nonreceptor environment—in vacuo, solvated, or crystalline—is a valid model for the receptor-bound structure of the drug. For TMP, the in vacuo and solvated minimized structures belonged to the same conformational family as the chicken liver DHFR-bound structure, as seen by RMS deviations (Table III), torsion angles (Table IV), and visual comparison (Figure 3). None of the minimized structures, however, accurately represents the conformation of TMP bound to *E. coli* DHFR. This demonstrates that, although some biologically significant conformations may be found by using minimization techniques, there may be other biologically active conformations. Note here that the technique of extracting snapshots along the dynamics trajectory and minimizing the structure at that point in order to obtain a new conformation would probably be unsuccessful for this molecule, since two distinctly different conformations, one from the small-molecule crystal and one from the *E. coli* DHFR complex, gave virtually identical conformations upon minimization in vacuo. In drug design, therefore, conformations away from minimum energy structures must be considered. For a molecule of the size of TMP, the allowable strain energy is ~6 kcal mol^{-1}. This is consistent with the 8 kcal mol^{-1} strain energy induced in cyclo(Ala-Pro-D-Phe)$_2$ in its crystal environment (Kitson & Hagler, 1988a). Conformational search by molecular dynamics without minimized snapshots (work in progress) has provided several conformations available to TMP at room temperature and may prove to be a preferred method for modeling. Similar considerations apply to any single conformation determined from experimental techniques in nonnative environments.

The neutral TMP crystal structure is most unlike either of the two enzyme-bound structures. In fact, the largest RMS deviation between the calculated structures (Table III) was found between the *E. coli* DHFR and small-molecule crystal structures. Thus, this particular TMP crystal would not be a reasonable model for TMP bound to either *E. coli* or chicken liver DHFR. The crystal environment determines the conformation of TMP, as seen by the three distinct conformations in TMP-related small-molecule crystals (entries 1–5, 6–8, and 9 in Table VII). Entry 9 (Table VII) would be a good model for TMP bound to the chicken liver enzyme, while entries 6–8 are close to TMP bound to the *E. coli* enzyme. In this case, the large number of TMP-related crystal structures gives a range of conformations accessible to this molecule. If there were only one structure, it could easily have a conformation unrelated to the enzyme-bound structure. This illustrates a major problem in the use of a crystal structure of an unbound inhibitor as the only template for the design of new drugs. Thus, where possible, it is advisable to use a variety of experimental and theoretical techniques to probe the accessible conformational states of a molecule in different environments. This then can provide a range of accessible states to be used as a basis for analogue design.

Conclusions

We have found that environment plays a major role in the conformation, energetics, and harmonic dynamics of the DHFR inhibitor TMP. Local differences in conformation, reflected in the differences in valence and torsion angles of various portions of the molecule, showed compensatory strain energies; i.e., conformations with lower torsion angle energies had higher valence angle energies and vice versa. The distributions of strain energies among the intramolecular degrees of freedom induced upon enzyme binding and crystallization emphasized the need to account for all terms in the valence energy, including angle deformations, in energy calculations.

Compensatory behavior was also seen between the intra- and intermolecular energies. The strain energies induced by the small-molecule crystal and the two DHFR complexes in the inhibitor were about the same (~6 kcal mol^{-1}), even though the TMP conformations were quite different in each. In the small-molecule crystal environment, the favorable in-

termolecular energies more than compensated for the intramolecular strain induced in the inhibitor by its surroundings. The DHFR systems had less favorable intermolecular energies, reflecting the less "ideal", enzyme-bound environment. The intermolecular energies were least favorable in the aqueous environment; less strain was induced, however, compensating for the lack of favorable intermolecular interactions.

Minimizations of small molecules are useful in many respects. Comparison of the minimized structure of a molecule in its crystal environment with the experimental structure provides a test of the potential parameters used. The geometry of the minimized TMP crystal structure was sufficiently close to that of the initial crystal structure to validate the usefulness of our potential parameters in modeling enzyme–substrate complexes. Minimizations with these parameters eliminated the significant deviations from standard geometry seen for TMP in the enzyme-bound crystallographic structures (Roberts et al., 1986). The in vacuo and solvated models gave structures in the same conformational family as TMP bound to chicken liver DHFR, but none of the unbound minimizations of TMP gave a structure related to that of TMP in the *E. coli* DHFR complex. The small-molecule crystal structure was not similar to either of the biologically active conformations, although the strain induced by the crystal lattice was the same as that induced by the enzymes. Examination of a large number of crystals of TMP derivatives, however, did provide structures related to both of the active conformations. Thus, neither a single local minimum nor a crystal structure alone will necessarily be a good template for the design of analogues based on conformational analysis. Instead, techniques that explore a range of low-energy conformations, such as molecular dynamics or systematic conformational searching, in conjunction with a variety of experimental studies may well be the optimal approach to explore the conformational space available to a molecule, and hence its possible binding modes.

ACKNOWLEDGMENTS

We thank Dr. D. H. Kitson for helpful discussions.

Registry No. TMP, 738-70-5.

REFERENCES

Avbelj, F., Moult, J., Kitson, D. H., James, M. N. G., & Hagler, A. T. (1990) *Biochemistry 29*, 8658–8676.

Baccanari, D. P., Daluge, S., & King, R. W. (1982) *Biochemistry 21*, 5068–5075.

Baker, B. R. (1970) in *Medicinal Chemistry (Part I)* (Burger, A., Ed.) pp 196–228, Wiley-Interscience, New York.

Bolin, J. T., Filman, D. J., Matthews, D. A., Hamlin, R. C., & Kraut, J. (1982) *J. Biol. Chem. 257*, 13650–13662.

Burchall, J., & Hitchings, G. H. (1965) *Mol. Pharmacol. 1*, 126–136.

Cauchy, A. L. (1847) *C. R. Hebd. Seances Acad. Sci. 25*, 536–538.

Cody, V. (1984) *Acta Crystallogr., Sect. C 40*, 1000–1004.

Dauber-Osguthorpe, P., Roberts, V. A., Osguthorpe, D. J., Wolff, J., Genest, M., & Hagler, A. T. (1988) *Proteins: Struct., Funct., Genet. 4*, 31–47.

Fletcher, R. (1970) *Comput. J. 13*, 317–322.

Fletcher, R., & Reeves, C. M. (1964) *Comput. J. 7*, 149–154.

Giuseppetti, G., Tadini, C., Bettinetti, G. P., Giordano, F., & La Manna, A. (1980) *Farmaco, Ed. Sci. 35*, 138–151.

Hagler, A. T. (1985) *Peptides (N.Y.) 7*, 213–299.

Kitson, D. H., & Hagler, A. T. (1988a) *Biochemistry 27*, 5246–5257.

Kitson, D. H., & Hagler, A. T. (1988b) *Biochemistry 27*, 7176–7180.

Koetzle, T. F., & Williams, G. (1976) *J. Am. Chem. Soc. 98*, 2074–2078.

Koetzle, T. F., & Williams, G. (1978) *Acta Crystallogr., Sect. B 34*, 323–326.

Makriyannis, A., & Fesik, S. (1982) *J. Am. Chem. Soc. 104*, 6462–6463.

Matthews, D. A., Bolin, J. T., Burridge, J. M., Filman, D. J., Volz, K. W., Kaufman, B. T., Beddell, C. R., Champness, J. N., Stammers, D. K., & Kraut, J. (1985a) *J. Biol. Chem. 260*, 381–391.

Matthews, D. A., Bolin, J. T., Burridge, J. M., Filman, D. J., Volz, K. W., & Kraut, J. (1985b) *J. Biol. Chem. 260*, 392–399.

Oberhänsli, W. E. (1970) *Helv. Chim. Acta 53*, 1787–1797.

Phillips, T., & Bryan, R. F. (1969) *Acta Crystallogr., Sect. A 25*, S200.

Roberts, V. A., Dauber-Osguthorpe, P., Osguthorpe, D. J., Levin, E., & Hagler, A. T. (1986) *Isr. J. Chem. 27*, 198–210.

Shimizu, N., & Nishigaki, S. (1982) *Acta Crystallogr., Sect. B 38*, 1834–1836.

Shimizu, N., Nishigaki, S., Nakai, Y., & Osaki, K. (1982) *Acta Crystallogr., Sect. B 38*, 2309–2311.

Swope, W. C., Andersen, H. C., Berens, P. H., & Wilson, K. R. (1982) *J. Chem. Phys. 76*, 637–649.